A Kinetic Model of the Hydrogen Assisted Selective Catalytic Reduction of NO with Ammonia over Ag/Al_2O_3

Stefanie Tamm and Louise Olsson
Competence Centre for Catalysis, Chalmers University of Technology, 412 96 Göteborg, Sweden

Chemical Reaction Engineering, Chalmers University of Technology, 412 96 Göteborg, Sweden

Sebastian Fogel
Haldor Topsøe A/S, Nymøllevej 55, 2800 Kgs. Lyngby, Denmark

Center for Individual Nanoparticle Functionality (CINF), Dept. of Physics, Technical University of Denmark, Fysikvej 307, 2800 Kgs. Lyngby, Denmark

Pär Gabrielsson
Haldor Topsøe A/S, Nymöllevej 55, 2800 Kgs. Lyngby, Denmark

Magnus Skoglundh
Competence Centre for Catalysis, Chalmers University of Technology, 412 96 Göteborg, Sweden

Applied Surface Chemistry, Chalmers University of Technology, SE-412 96 Göteborg, Sweden

DOI 10.1002/aic.14170
Published online July 15, 2013 in Wiley Online Library (wileyonlinelibrary.com)

A global kinetic model which describes H_2-assisted NH_3-SCR over an Ag/Al_2O_3 monolith catalyst has been developed. The intention is that the model can be applied for dosing NH_3 and H_2 to an Ag/Al_2O_3 catalyst in a real automotive application as well as contribute to an increased understanding of the reaction mechanism for NH_3-SCR. Therefore, the model needs to be simple and accurately predict the conversion of NO_x. The reduction of NO is described by a global reaction, with a molar stoichiometry between NO, NH_3 and H_2 of 1:1:2. Further reactions included in the model are the oxidation of NH_3 to N_2 and NO, oxidation of H_2, and the adsorption and desorption of NH_3. The model was fitted to the results of an NH_3-TPD experiment, an NH_3 oxidation experiment, and a series of H_2-assisted NH_3-SCR steady-state experiments. The model predicts the conversion of NO_x well even during transient experiments. © 2013 American Institute of Chemical Engineers *AIChE J*, 59: 4325–4333, 2013
Keywords: NH_3-SCR, NO_x reduction, H_2, global kinetic model, Ag/Al_2O_3

Introduction

The reduction of nitrogen oxides (NO_x) in an oxidizing environment of the exhaust of a diesel or lean burn gasoline engine is one of the most challenging tasks for the catalytic converter in a vehicle. Moreover, exhaust gas temperatures have decreased during the last years due to more efficient utilization of the fuel in the engine. This leads to a demand of catalysts which are active for NO_x reduction below 200°C. Nitrogen oxides can be efficiently reduced by selective catalytic reduction with ammonia (NH_3-SCR). Different copper and iron exchanged zeolites have been studied for this application during the last decades.[1–4] More recently it was shown that also Ag/Al_2O_3 shows very good activity for the NH_3-SCR reaction, reaching close to 100% NO_x conversion at 200°C.[5] In contrast to the zeolite-based catalysts, hydrogen is essential for efficient NH_3-SCR over Ag/Al_2O_3.[5–7] Although the H_2-effect is known from the SCR reaction with hydrocarbons over Ag/Al_2O_3[8–10] this effect is still not fully understood and a number of different mechanisms have been proposed, e.g., an increase of the number of active species,[11,12] reduction of silver,[9,13,14] increased amount of surface species[15–17] and removal of nitrates.[13,17–21] Recently, we showed that the presence of H_2 facilitates the oxidation of nitrites to nitrates and, moreover, influences how the nitrates preferentially are bound to the surface.[22] In the presence of H_2, there is a defined ratio between NO : NH_3 : H_2 of 1:1:2 at low temperatures, where no unselective oxidation of NH_3 and H_2 occurs.[23] This ratio is explained by hydrogen selectively removing single-oxygen atoms from the active silver sites, freeing the sites for NO and NH_3 adsorption.[23]

Based on the proposed reaction mechanism, kinetic models have been developed. Several detailed kinetic models have been developed for a variety of different SCR catalysts to increase the understanding of the reaction mechanism.[2,19,24–27] Moreover, such a model can be used as a tool in the

Correspondence concerning this article should be addressed to L. Olsson at Louise.Olsson@chalmers.se.

development of the complex exhaust gas after-treatment system of a vehicle, which may contain additional catalysts, for example, a diesel oxidation catalyst (DOC). Finally, a model is needed for the dosing strategy of the reducing agent. This model needs to accurately predict the NO_x conversion as a function of the temperature, the surface coverage of important species, especially the reducing agent, and the concentration in the gas phase of the reducing agent. Furthermore, a model of H_2-assisted NH_3-SCR over Ag/Al_2O_3 needs even to describe the H_2 concentration.

In the literature there are several kinetic models for Ag/Al_2O_3 catalysts.[19,28–30] However, these models all describe hydrocarbon SCR (HC—SCR). The objective of this study is to develop a simple global kinetic model for H_2-assisted NH_3-SCR over an Ag/Al_2O_3 catalyst, which can be used for the dosing strategy of NH_3 and H_2. This model is based on the knowledge available for the reaction mechanism and on flow reactor experiments performed using a monolith catalyst, where the concentrations of all important gaseous compounds are varied. Most of the experimental results have already been reported previously.[23] However, to keep the model simple, only the most important reactions are included in the model and also the number of included species is limited.

Experimental Methods

A presulfated Ag/Al_2O_3 monolith catalyst with 6 wt% silver was used in the study. A higher amount of silver is needed to compensate for the loss of activity caused by sulfate formation. A catalyst in a real application will continuously be exposed to small amounts of sulfur from the fuel and lubricants. By presulfation we account for this sulfur exposure. More details about the preparation and properties of the catalyst can be found elsewhere.[23] Catalytic activity tests were performed in a horizontally mounted quartz tube flow reactor designed for monolithic catalyst samples. The quartz tube was externally heated by a heating coil and the monolith was placed in the end of the heated zone. The temperature of the reactor was measured inside a center channel of the monolith sample and controlled in the gas stream 10 mm before the monolith. Gases were supplied by separate mass flow controllers and water was added by a controlled evaporation and mixing system (all Bronkhorst Hi-Tech). The outlet gas composition was continuously analyzed using a gas phase FTIR spectrometer (mks-instruments, MultiGas2030) with the gas cell heated to 191°C and by mass spectrometry (Hiden HPR-20 QIC).

All activity tests were performed with a total flow of 3,500 mL/min, resulting in a GHSV of 33,100 h^{-1}. The fresh catalyst was first activated for 5 min at 670°C in 5% water and then degreened in 250 ppm NO, 250 ppm NH_3, 10% O_2 and 5% H_2O in Ar at 600°C for 3 h. In each subsequent experiment the sample was initially pretreated in a flow of 10% O_2 in Ar at 500°C for 20 min. Afterward, the catalyst was cooled in 5% water in Ar to 70°C, where it was exposed to the reaction mixture for 40 min. Then, the temperature was increased in 8 steps at 20°C/min to 500°C (100, 150, 200, 250, 300 and 400°C). Each step lasted at least 20 min to obtain steady-state conditions. For temperature programmed desorption (TPD) experiments, the catalyst was cooled to 100°C in 5% water in Ar after the pretreatment. At this temperature, the catalyst was exposed to the gas mixture for 60 min followed by flushing of the catalyst for 30 min at the same temperature. Subsequently, the temperature was raised by 20°C/min to 600°C and desorption of species was monitored. More details on the experiments can be found in a previous publication.[23]

Model

Kinetic model

The kinetic model was developed by successively expanding the initial model with more reactions. As a first step, the adsorption and desorption of NH_3 were modeled using an NH_3-TPD experiment. In this experiment, 250 ppm NH_3, 10% O_2 and 5% H_2O were present during the NH_3 adsorption step and only Ar in the following temperature ramp. Experiments have shown that the presence of O_2 or H_2 has no significant influence on the adsorption of NH_3 and these compounds are, therefore, not included in the model. The elementary steps and reactions included in the model are presented in Table 1. According to the model, ammonia adsorbs on two different sites, S1 and S2 with different adsorption energies.

Previously, we have shown by diffuse reflectance IR Fourier transform spectroscopy (DRIFTS) that the predominant surface species during H_2-assisted NH_3-SCR conditions are NH_x species.[6] Although we know that even nitrates and nitrites exist on the surface during the reaction, we chose here to only include NH_3 adsorption in the model, since the purpose with the model is to use it for dosing of the reducing agents. Therefore, we aim for a simple model and fast calculations.

In the next step, oxidation of NH_3 with O_2 was modeled. Adsorbed NH_3 on the S1 site reacts with O_2 to N_2, reaction 5, or to NO, reaction 6 in Table 1. Reaction 5 (NH_3 oxidation to N_2) is needed to describe the formation of N_2 during NH_3 oxidation in the absence of H_2. In the presence of H_2, N_2 formation could also be formed by reaction 7 (SCR). Finally, the H_2-assisted NH_3-SCR reaction was modeled as one global reaction with a stoichiometry between NO, NH_3 and H_2 of 1:1:2. The stoichiometry has been established in a previous article on the basis of flow reactor experiments.[23] Moreover, the unselective oxidation of H_2 with O_2 is added to the model (reaction 8 in Table 1). In addition to production of NO and N_2, formation of NO_2 and N_2O can be expected as side products during H_2-assisted NH_3-SCR over Ag/Al_2O_3 catalysts. However, over the presulfated Ag/Al_2O_3 sample, which was used for the reactor experiments, no formation of N_2O was observed under any reaction conditions in the presence of water.[23] At 200°C, the formation of some NO_2 was observed.[23] However, since the NO_2 concentration never exceeded 15 ppm and, moreover, occurred only at that specific temperature, reactions including NO_2 and N_2O were omitted in the model.

Table 1. Reactions Included in the Model

Reaction number	Reaction
r1	$NH_3 + S1 \rightarrow NH_3\text{-}S1$
r2	$NH_3\text{-}S1 \rightarrow NH_3 + S1$
r3	$NH_3 + S2 \rightarrow NH_3\text{-}S2$
r4	$NH_3\text{-}S2 \rightarrow NH_3 + S2$
r5	$2\ NH_3\text{-}S1 + 1.5\ O_2 \rightarrow N_2 + 3\ H_2O + 2\ S1$
r6	$2\ NH_3\text{-}S1 + 2.5\ O_2 \rightarrow 2NO + 2H_2O + 2\ S1$
r7	$2\ NO + 2\ NH_3\text{-}S1 + 2.5\ O_2 + 4\ H_2 \rightarrow 2\ N_2 + 7\ H_2O + 2\ S1$
r8	$2\ H_2 + O_2 \rightarrow 2\ H_2O$

Table 2. Reaction Rates, Pre-Exponential Factors and Activation Energies used in the Model

Reaction number	Reaction rate	Pre-exponential factor A	Activation energy E_a [J/mol]
r1	$r1 = k_1 \cdot c_{NH3} \cdot (1\text{-}\theta_{S1})$	355[a]	0
r2	$r2 = k_2 \cdot \theta_{S1}$	$3.5 \cdot 10^{8}$ [b]	$8.3 \cdot 10^{4}$ [d]
r3	$r3 = k_3 \cdot c_{NH3} \cdot (1\text{-}\theta_{S2})$	2030[a]	0
r4	$r4 = k_4 \cdot \theta_{S2}$	$2.0 \cdot 10^{9}$ [b]	$6.3 \cdot 10^{4}$ [d]
r5	$r5 = k_5 \cdot \theta_{S1}$	$2.5 \cdot 10^{8}$ [b,e]	$1.43 \cdot 10^{5}$ [d]
r6	$r6 = k_6 \cdot \theta_{S1}$	$4.5 \cdot 10^{12}$ [b,e]	$2.09 \cdot 10^{5}$ [d]
r7	$r7 = k_7 \cdot c_{NO} \cdot \theta_{S1} \cdot c_{H2}$	$1.49 \cdot 10^{14}$ [b,e]	$1.20 \cdot 10^{5}$ [d]
r8	$r8 = k_8 \cdot c_{H2}$	$1.18 \cdot 10^{10}$ [b,e]	$1.20 \cdot 10^{5}$ [d]

[a] $m^3/(s \cdot kg_{cat})$, calculated by kinetic gas theory
[b] mol/(s·kg cat)
[c] calculated by transition state theory
[d] fitted for the model

Parameters in the kinetic model

The expressions used for the reaction rates for each reaction are presented in Table 2 and the corresponding rate constants in the reaction rates are described by the Arrhenius equation

$$k_j = A_j(T) \cdot e^{\frac{-E_{a,j}}{R \cdot T}} \tag{1}$$

Temperature dependence of the pre-exponential factors is neglected in the model. To decrease the correlation between parameters in the model, some parameters were determined in advance. It was shown that many adsorption reactions are nonactivated or have low-activation energies.[31] Therefore, the activation energy for adsorption of NH_3 on both adsorption sites (S1 and S2) is set to 0 kJ/mol, which is in line with other kinetic models.[26,32] The pre-exponential factors for the adsorption reactions, A_{ads} (A_1 and A_3) were determined by using kinetic gas theory[33]

$$A_{ads} = \frac{N_A \cdot R \cdot T}{(2 \cdot \pi \cdot M \cdot R \cdot T)^{0,5}} \cdot A \cdot N_{cat} \cdot S(0) \tag{2}$$

Here, a reference temperature of 300°C was used. Pre-exponential factors for reactions and desorption are typically in the range of $10^{11}-10^{19}$ s^{-1}.[33] Here we used for the pre-exponential factors of the desorption reactions r2 and r4 according to transition state theory

$$\frac{k_B \cdot T}{h} = 10^{13} s^{-1} \tag{3}$$

This value is adjusted by the number of sites (N_{cat}) to obtain the unit $m^3/(s \cdot kg_{cat})$. All pre-exponential factors and activation energies are listed in Table 2.

Reactor model

The monolith catalyst is modeled as five continuously stirred-tank reactors in series. The number of tanks is a compromise between computational time and accuracy. In the mass balance of the gases in each tank the difference between the molar flow from the previous tank and the flow to the next tank is equal to the mass transport from the gas bulk to the catalyst surface

$$F_{i,k-1} - F_{i,k} = k_{c,i,k} \cdot A_k \cdot \left(c_{g,i,k} - c_{s,i,k}\right) \tag{4}$$

All channels of the monolith are assumed to be identical. The mass transport from the bulk to the catalyst surface is equal to the adsorption, desorption and reactions occurring on the catalyst surface

$$k_{c,i,k} \cdot A_k \cdot \left(c_{g,i,k} - c_{s,i,k}\right) = \sum\nolimits_j v_{i,j} \cdot r_{j,k} \cdot m_{wc,k} \tag{5}$$

Moreover, it is assumed that there are no radial concentration gradients, and no axial diffusion. Axially changes in the gas concentration over the catalyst are modeled by the number of tanks. Any mass-transfer limitations in the washcoat are neglected, and the mean surface coverage in each tank is used to model the surface reactions. The changes of the amount of one type of species on the catalyst surface are equal to the sum of all reaction of this species

$$N_{cat} \frac{\partial \theta_{i,k}}{\partial t} = \sum\nolimits_j v_{i,j} \cdot r_{j,k} \tag{6}$$

The mass transfer from the bulk in the gas phase to the catalyst surface is modeled by the film model, where the mass transfer coefficient $k_{c,i,k}$ is calculated from the Sherwood number

$$k_{c,i,k} = \frac{Sh \cdot D}{d_{channel}} \tag{7}$$

Where the diffusivity D is calculated according to

$$D = D_{ref} \cdot \left(\frac{T_{cat}}{T_{ref}}\right)^{1.75} \tag{8}$$

The reference diffusion coefficients were obtained from the Fuller correlation[34] and have values of 9.71×10^{-5} m^2/s for NO, 8.31×10^{-5} m^2/s for O_2, 34.12×10^{-5} m^2/s for H_2, and 9.35×10^{-5} m^2/s for NH_3 at a reference temperature of 400°C. The Sherwood number Sh was here calculated from

$$Sh = 2.7652 \cdot (1 + 0.03349 \cdot Gz) \tag{9}$$

Where the Graz number is obtained from

$$Gz = \frac{d_{channel}^2 \cdot v}{L_{monolith} \cdot D} \tag{10}$$

and v is the linear gas velocity. At all places in the monolith isothermal conditions are used since the temperature difference between the gas in the inlet of the monolith and the temperature in the monolith is less than 18.5°C at all studied temperatures. The maximum in temperature difference occurred between 300 and 400°C, where most of the H_2 is combusted. The temperature used in the model is the monolith temperature.

Results and Discussion

The conversion of NO increased slowly with the number of experiments as shown in Figure 1. In a previous investigation,

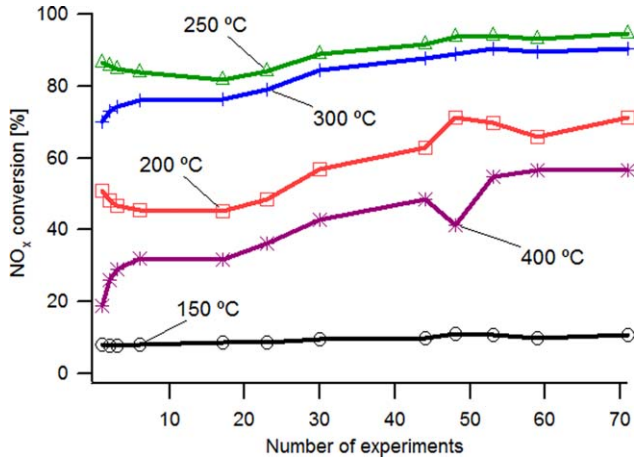

Figure 1. Conversion of NO_x as a function of experiment number at different temperatures.

[Color figure can be viewed in the online issue, which is available at wileyonlinelibrary.com.]

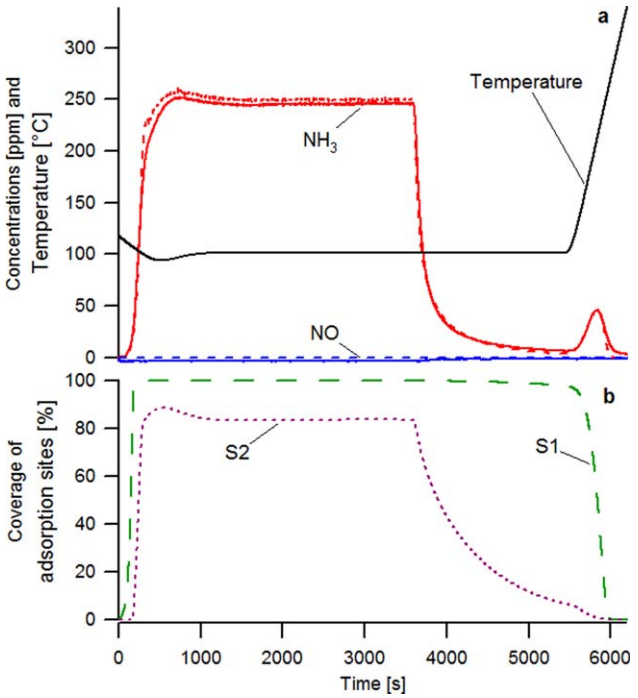

Figure 2. Measured (solid lines) and calculated (broken lines) concentrations and temperature (a), calculated coverage of S1 and S2 (b) during NH_3-TPD.

Conditions: 250 ppm NH_3, 10% O_2 and 5% H_2O in Ar for 60 min at 100°C, 5% H_2O in Ar for 30 min at 100°C, temperature ramp in 5% H_2O in Ar, 20°C/min, GHSV = 33100 h^{-1}. [Color figure can be viewed in the online issue, which is available at wileyonlinelibrary.com.]

this increase has been explained by a gentile aging during the pretreatments and a part of each experiment at 500°C.[23] Each experiment consisted of activity tests at steady-state conditions between 150 and 500°C. For the modeling, a change in the conversion over time is a major challenge. Most of the experiments, which were included in the development of the model, were performed between the 17th and the 44th experiments. Between these experiments, the NO_x conversion increased in the entire temperature range of the experiments. The most pronounced changes are observed at 200 and 400°C as shown in Figure 1. However, all experiments, in which the H_2 concentration was varied, were performed consecutively. The same is true for the variation of the NO and the variation of the NH_3 concentration. This procedure minimized the changes due to aging so that the aging does not need to be taking into account in the parameter fitting of the model. With these measures taken, a robust model was developed since it predicts the validation experiments well, which were performed after the 71st experiment.

Ammonia Temperature Programmed Desorption (NH_3-TPD) Experiments

An NH_3-TPD experiment was used to model the NH_3 adsorption and desorption from the catalyst, and to determine the number of sites on which the reactions take place. As shown in Figure 2a, the model describes all features observed in the NH_3-TPD well. For a good fit between experiment and model, two different adsorption sites were included in the model. One strong adsorption site, S1, and one weaker adsorption site, S2. The modeling results gave that the concentration of S1 and S2 sites is 0.04 and 0.2 $mol/kg_{catalyst}$, respectively. As shown in Figure 2b, the strong adsorption site, S1, reaches full coverage fast due to the low concentration of this type of sites. The coverage of S2 starts to increase when the S1 sites are completely covered but reaches only 80% coverage at 100°C. The coverage of the S2 site is here very sensitive to the temperature and accounts for the small increase in NH_3 concentration, when the temperature increases from 98 to 100°C after about 1000 s. Moreover, the ammonia on the S2 site desorbs slowly at 100°C and gives rise to the tailing of the NH_3-signal, which is observed after the NH_3 supply is switched off. During the 30 min between NH_3 has been switched off and the start of the temperature ramp, the coverage of the S2 site decreases steadily. However, at the beginning of the temperature ramp, there is still some NH_3 adsorbed on S2. The ammonia coverage of S1 is constant during the flushing and drops during the temperature ramp. Since the catalyst consists of alumina supported silver species, it is possible to attribute silver and alumina sites to S1 and S2, respectively. However, according to Knözinger and Ratnasamy,[35] and Digne et al.[36] there are at least four different types of OH-groups with different properties on which molecules can adsorb on the alumina. Moreover, there will be differences depending on if a molecule adsorbs on a silver species or in the interface between a silver cluster and the alumina support.[37] However, in this model we used S1 and S2 sites in order to make the model simpler. In kinetic models, it is common to use coverage dependent activation barriers for desorption. The reason is either repulsive interaction between species or adsorption sites with a range of strength. For example Wilken et al.[38], and Saha and Deng[39] determined the coverage dependent heats of adsorption over Cu-BEA and alumina, respectively. Sjövall et al.[40] used the coverage dependent activation energies according to

$$E_a = E_a(0) \cdot (1 - a_i \cdot \theta_i) \tag{11}$$

In this model, however, the best fit of the model to the experimental data is achieved when the activation energies for desorption from both sites (S1 and S2) are independent

of the coverage. Since we in this study use two adsorption sites, we also consider the effect of different strength of the sites. In the study by Wilken et al.[38] only one adsorption site was used.

Ammonia oxidation

Figure 3a shows the concentrations of NH_3 and NO during NH_3 oxidation at different temperatures. Ammonia is adsorbed on the catalyst surface at 70°C and each time the temperature is increased some NH_3 desorbs up to 400°C. This is also the temperature, where NH_3 oxidation starts. Significant concentrations of NO, however, are only observed at 500°C. Formation of NO_2 or N_2O does not occur during the experiment. The part of the experiment without NH_3 oxidation is, thus, a validation of the parameters for NH_3 adsorption and desorption. There is a difference between the experimental and predicted results from the model for the NH_3 adsorption at 70°C, and the desorption peaks during the temperature increase to 100 and 150°C as shown in Figure 3a. This difference occurs since the parameters for NH_3 adsorption were obtained from a TPD experiment performed at 100°C. However, above 150°C where the catalyst is active for NO_x reduction, the model describes desorption of NH_3 well. Figure 3b shows the calculated surface coverages of S1 and S2, which decrease stepwise with each temperature increase. Due to NH_3 being present in the gas phase during the entire experiment, the model predicts some adsorbed NH_3 on S2 for temperatures below 250°C and on S1 below 400°C.

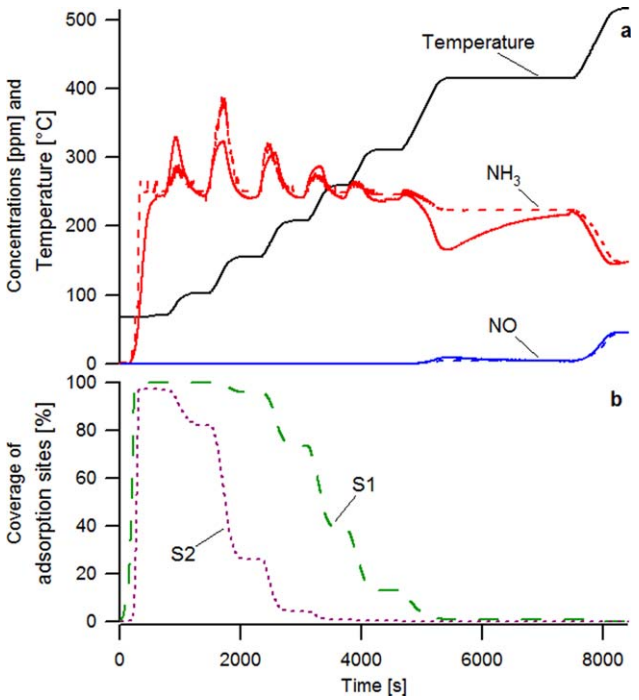

Figure 3. Oxidation of ammonia at different temperatures between 70 and 500°C, measured (solid lines) and calculated (broken lines) concentrations during NH_3 oxidation and temperature (a), and calculated surface coverage of S1 and S2 (b).

Conditions: 250 ppm NH_3, 10% O_2 and 5% H_2O in Ar, GHSV = 33100 h^{-1}. [Color figure can be viewed in the online issue, which is available at wileyonlinelibrary.com.]

At 400°C, oxidation of NH_3 starts but only trace amounts of NO are observed. Although N_2 has not directly been measured it is obvious from an N-balance that the major part of the oxidized NH_3 forms N_2. At 500°C, substantial amounts of NO are formed and also the amount of formed N_2 increases. In the model, two reactions are introduced to describe NH_3 oxidation, i.e., the oxidation of NH_3 to N_2 (r5) and the oxidation of NH_3 to NO (r6). Formation of N_2O or NO_2 is not included, since these components were not observed in the experiments. With these assumptions the model describes the steady-state conditions during the oxidation of NH_3 well. However, the temporary decrease of the NH_3 concentration when increasing the temperature from 300 to 400°C cannot be described by the model as shown in Figure 3. In a previous publication, this temporary decrease of the NH_3 concentration was tentatively explained by a change in the oxidation state of the silver.[23] This phenomenon is more pronounced in the absence than in the presence of hydrogen and during the first NH_3 oxidation experiment succeeding an SCR experiment. A possible explanation for the different behavior in the absence and the presence of hydrogen is the fact, that silver oxides decomposes to metallic silver around 300°C in inert atmosphere.[41] Hydrogen as a reducing agent will clearly influence this process. Moreover, the oxidation of NH_3 is impeded by H_2 and increases with increasing O_2 concentration.[23] Since the oxidation of NH_3 occurs during NH_3-SCR conditions only at 500°C, the dependencies on O_2 and H_2 are not included in the model to keep the model simple. Finally, it is interesting to note, that the formation of NO starts at the same temperature at which the model predicts that all NH_3 has desorbed from the surface. The co-occurrence of the surface coverage reaching zero and the start of the temporary decrease in the NH_3 concentration supports the explanation by the change in the oxidation state of the silver.

Hydrogen-assisted ammonia-SCR

The Ag/Al_2O_3 catalyst is very active for NO_x reduction with NH_3 in the presence of H_2 as shown in Figure 4. Significant conversion of NO is observed from 150°C and a maximum of 93% is reached at 250°C. At higher

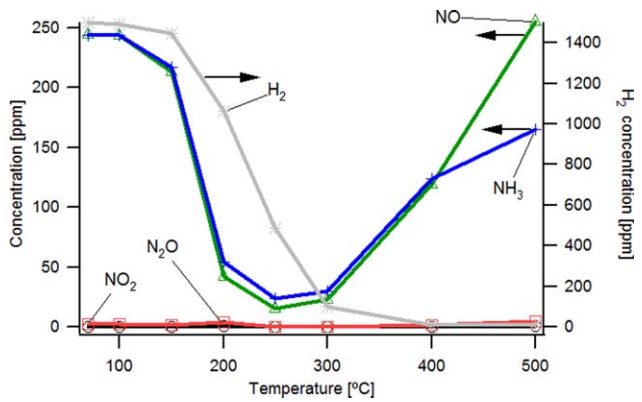

Figure 4. Concentrations of all relevant gases during H_2-assisted NH_3-SCR under steady-state conditions.

Experimental conditions: 250 ppm NO, 250 ppm NH_3, 1500 ppm H_2, 10% O_2, 5% H_2O in Ar.[Color figure can be viewed in the online issue, which is available at wileyonlinelibrary.com.]

temperatures, the NO concentration is higher. At 500°C, the NO concentration after the catalyst is higher than in the inlet due to oxidation of NH_3 to NO. At all other studied temperatures the NO and NH_3 concentrations follow each other closely and a ratio of one converted NO by one converted NH_3 has been established in a previous publication.[23] Moreover, NO, NH_3 and H_2 conversions start all at 150°C. All hydrogen is consumed at 400°C, where the NO concentration significantly increases, indicating that the lack of hydrogen limits the conversion of NO above 300°C. However, Ag/Al_2O_3 is not active for NO_x reduction with only H_2 as reducing agent.[6,23] In a previous publication it was shown that there is a ratio between consumed NO and consumed H_2 of 1:2 below 250°C.[23] Above this temperature, unselective oxidation of H_2 becomes increasingly important. As during the oxidation of NH_3, the amounts of formed NO_2 and N_2O are extremely low. These gases are, therefore, not included in the model. Moreover, the reduction of NO with NH_3 and H_2 to N_2 and H_2O is modeled as a single global reaction with a stoichiometry of NO: NH_3 : H_2 is equal to 1:1 : 2

$$2\,NO + 2\,NH_3 + 2.5\,O_2 + 4\,H_2 \rightarrow 2\,N_2 + 7\,H_2O$$

Variation of the hydrogen concentration

The conversion of NO is sensitive to the concentration of H_2. As shown by the markers in Figure 5a and b, the NO and NH_3 concentrations decrease in a ratio of 1:1 with increasing H_2 concentration at a fixed temperature, i.e., the NO_x conversion increases with increasing H_2 concentrations in the feed. Figure 5c shows the concentration of H_2 as a function of the temperature. Although, there is a large difference in the feed concentration of H_2, hydrogen conversion starts at 150°C, independently of the inlet concentration. Moreover, complete H_2 conversion is in all experiments observed at 400°C, and at intermediate temperatures the conversion is independent of the inlet H_2 concentration within the studied concentration interval. The model captures all these features well as shown by the comparison of the model (lines) and the experimental data (markers) in Figure 5. In addition to the SCR reaction an unselective oxidation reaction of H_2 is included to account for the higher H_2 consumption above 250°C. However, there are some minor discrepancies. The model overestimates the NH_3 oxidation at 500°C. This could be resolved by adding that H_2 impedes the oxidation of NH_3 to the model, but would complicate the model. Moreover, the model somewhat overestimates the NO_x conversion for 250 and 500 ppm H_2. The model predicts that the surface coverage of S2 is independent of the inlet concentration of H_2. In contrast to S2, the surface coverage of S1 decreases with increasing concentration in the inlet H_2 concentration between 200 and 300°C as shown in Figure 5d. This dependency of the surface coverage on the H_2 concentration is caused by differences in the actual NH_3 concentrations in the gas phase. In the context of the NH_3-TPD, we attributed S1 and S2 to sites on silver and alumina, respectively. However, it has been shown that alumina is necessary for the SCR-reaction over Ag/Al_2O_3.[6] Therefore, an unambiguous assignment of S1 and S2 to any physical sites on the catalyst is not possible.

Variation of the NO concentration

In addition to the variation of the H_2 concentration also the NO concentration was varied keeping all other gas concentrations constant as shown in Figure 6. The NO conversion increases with decreasing inlet NO concentration due to a higher ratio between NO and the reducing agents. The model describes this phenomenon very well. Only at 200°C, the model overestimates the NO and NH_3 conversion. Moreover, the model predicts that the coverage of the S2 site is independent of the NO concentration, while the coverage of the S1 site is higher with 125 ppm NO in the feed than with 250 or 375 ppm NO as shown in Figure 6d. This is reasonable, since the same trend is observed for the NH_3 concentration in the gas phase.

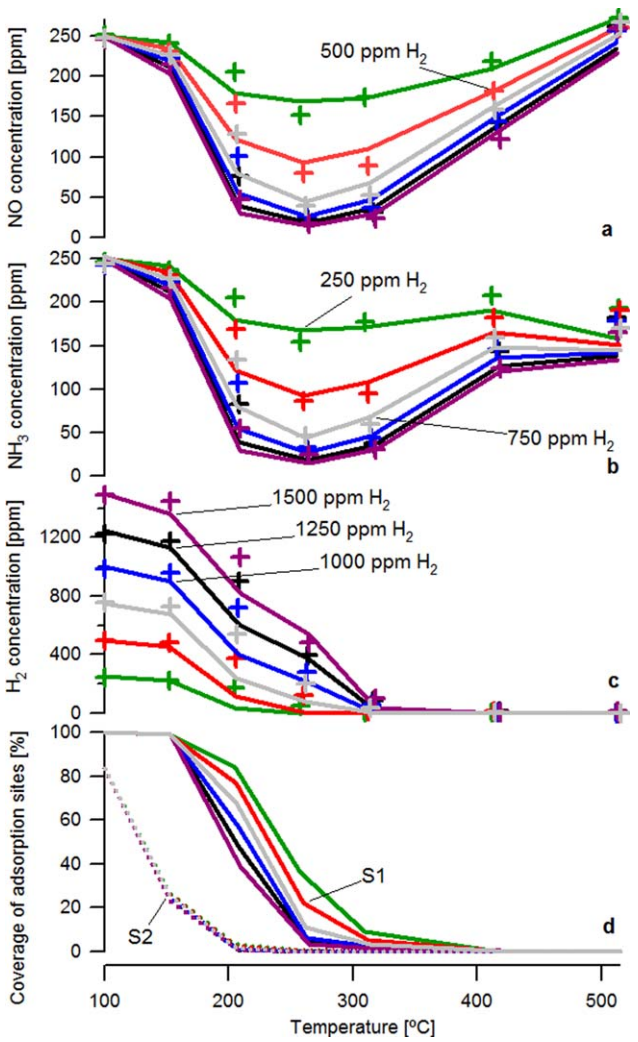

Figure 5. Concentrations of NO (a), NH_3 (b), and H_2 (c) during H_2-assisted NH_3-SCR with different concentrations of H_2 during steady-state conditions between 100 and 500°C.

Experimental results are represented by points and calculated concentrations by the model as lines. Experimental conditions: 250 ppm NO, 250 ppm NH_3, 250–1500 ppm H_2, 10% O_2, 5% H_2O in Ar. Calculated surface coverage of S1 (solid line) and S2 (broken line) (d). [Color figure can be viewed in the online issue, which is available at wileyonlinelibrary.com.]

Variation of the NH_3 concentration

The concentration of NH_3 has also been varied as another important parameter for H_2-assisted NH_3-SCR. As shown in Figure 7a and b, lowering the NH_3 concentration to a molar

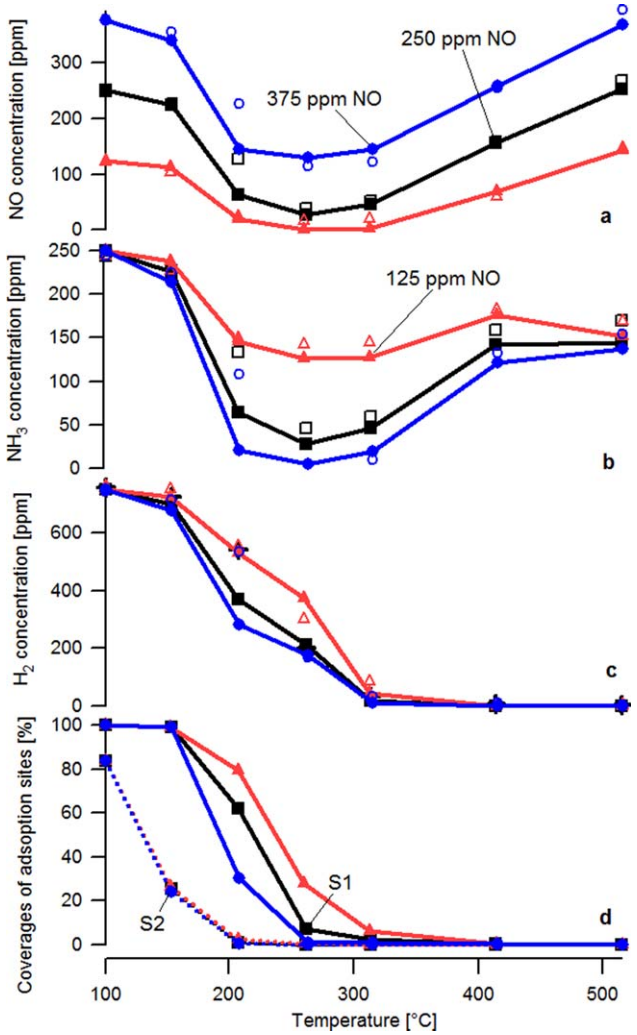

Figure 6. Concentrations of NO (a), NH_3 (b) and H_2 (c) during H_2—assisted NH_3-SCR with different concentrations of NO during steady state conditions between 100 and 500°C.

Experimental results are represented by markers and calculated concentrations by the model as lines. Experimental conditions: 125, 250 or 375 ppm NO, 250 ppm NH_3, 750 ppm H_2, 10% O_2, 5% H_2O in Ar. Calculated surface coverage of S1 (solid line) and S2 (broken line) (d). [Color figure can be viewed in the online issue, which is available at wileyonlinelibrary.com.]

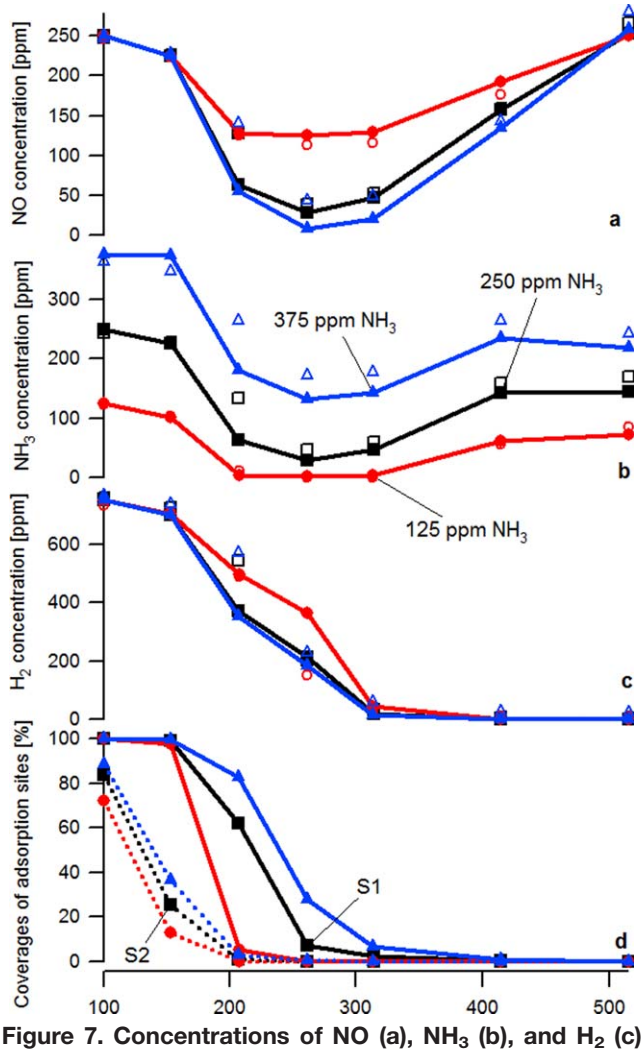

Figure 7. Concentrations of NO (a), NH_3 (b), and H_2 (c) during H_2-assisted NH_3-SCR with different concentrations of NH_3 during steady state conditions between 100 and 500°C.

Experimental results are represented by markers and calculated concentrations by the model as lines. Experimental conditions: 125, 250 or 375 ppm NH_3, 250 ppm NO, 750 ppm H_2, 10% O_2, 5% H_2O in Ar. Calculated surface coverage of S1 (solid line) and S2 (broken line) (d). [Color figure can be viewed in the online issue, which is available at wileyonlinelibrary.com.]

ratio of one NH_3 to two NO in the feed limits the NO conversion. However, increasing the ratio of NH_3 to NO above 1:1 is not beneficial for the NO conversion. This is unexpected after the results from the variation of the NO concentration. To explain this phenomenon it is important to notice, that the ratio between NH_3 and NO as well as the ratio between NH_3 and H_2 changes when changing the NH_3 concentration and keeping all other parameters constant. It can, thus, be concluded that the H_2 concentration limits the NO_x conversion under these conditions. The model describes the NO_x conversions with different inlet NH_3 concentrations well. Due to different NH_3 concentrations in the outlet, the model also predicts different coverages on the two different adsorption sites. The dependence on the NH_3 concentration of the S2 adsorption site was not seen when varying the concentrations of H_2 or NO (Figure 5d and Figure 6d). In these experiments, no major NH_3 conversion occurred below 200°C, where a significant coverage of the S2 site is predicted. Thus, the similar coverages in the previous experiments are due to similar NH_3 outlet concentrations.

Validation of the model

The model was validated against three additional transient experiments, which were not included in the development of the model. These experiments were conducted at constant temperature (150, 200 and 250°C) where the supply of NO, H_2 and NH_3 to the feed separately was switched on and off after one long step with all compounds in the feed as shown in Figure 8a. All following steps lasted for 5 min. The model was developed with steady-state experiments, with exception for the NH_3-TPD experiment. In the validation experiments with short steps, adsorption and desorption have a larger impact on the conversion of all gases. Figure 8 shows the transient experiment performed at 200°C; the temperature, at

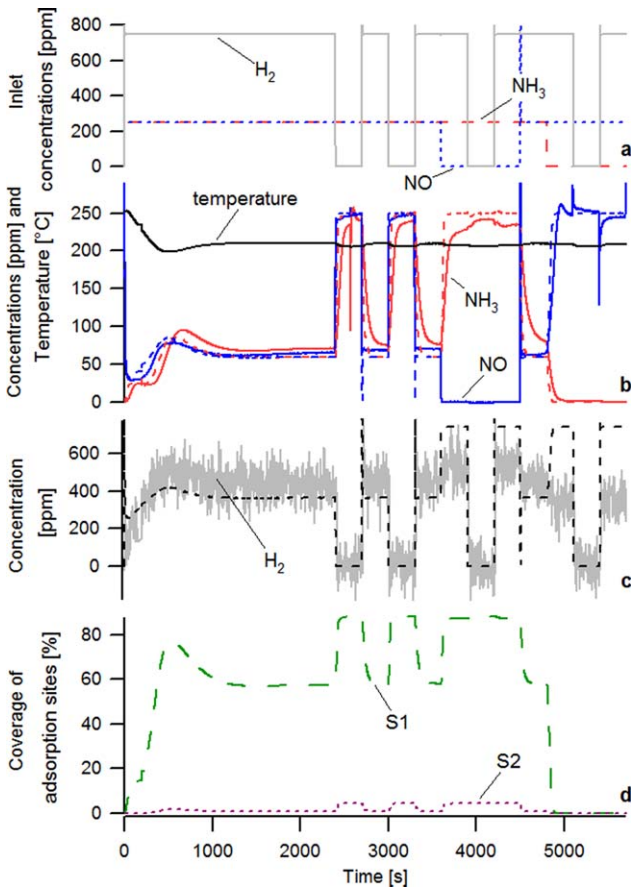

Figure 8. Feed gas composition (a) Experimental data (broken line) and calculated concentrations by the model (solid line) during a transient experiment switching H_2, NO and NH_3 on and off at 200°C (b,c).

Calculated surface coverage during the experiment (d).[Color figure can be viewed in the online issue, which is available at wileyonlinelibrary.com.]

which the fit between model and experiment is the worst. The light-off of the SCR-reaction occurs between 150 and 200°C. Therefore, the calculated concentrations are at 200°C especially sensitive to the parameters. In addition, the gradient of the conversion is steepest close to the light-off, which is also the case at 200°C. A small error in the temperature measurement will in this temperature region cause a clear deviation between the model and the experiment. Despite this difference during the fitting, the model describes the NO_x conversion of this transient experiment very well. The model somewhat underestimates the adsorption and desorption of NH_3 when the supply of different gas components is switched on and off. In addition, the conversion of hydrogen is somewhat inaccurate in the absence of ammonia in the last part of the experiment in Figure 8. This is due to the fact that at 200°C hydrogen is mainly consumed in the SCR reaction (r7) in the model. This reaction does not occur in the absence of NH_3. At 200°C, the model predicts very low-surface coverage's, between 0–5% for S2 and about 70% for S1 during NH_3-SCR. When the hydrogen supply is switched off from the feed, the NH_3 coverage of S1 increases and reaches close to 90%. The same coverage of S1 is also predicted when both the supply of NO and H_2 are switched off from the feed. In the presence of H_2, NH_3 and O_2, however, the coverage is somewhat lower. This is interesting to note, since the NH_3 concentration decreased somewhat under these conditions in the experiment, but this detail is not reproduced by the model.

Conclusions

A global kinetic model which describes hydrogen-assisted selective catalytic reduction of NO_x with NH_3 over Ag/Al_2O_3 has been developed. The intention is that the model can be applied for dosing NH_3 and H_2 for a Ag/Al_2O_3 catalyst in a real automotive application. For this purpose, it is important that the model is simple to allow for fast calculations and, at the same time, accurately predicts the conversion of NO_x. To achieve this goal, the model includes the adsorption and desorption of NH_3 on two adsorption sites with different adsorption properties. Moreover, oxidation of NH_3 to N_2 and NO, and unselective oxidation of H_2 to water are included. The reduction of NO is described by a global reaction, with a stoichiometry between NO, NH_3 and H_2 of 1:1:2. The parameters of the model were obtained by fitting of an NH_3–TPD experiment in the presence of O_2, an NH_3 oxidation experiment with 10% O_2 in the adsorption step, and a series of H_2—assisted NH_3-SCR steady-state experiments in which the concentrations of H_2, NO and NH_3 were varied. With the obtained parameters and a set of six reactions it is possible to predict the conversion of NO_x well even during transient experiments.

Acknowledgments

This work is financially supported by the Danish Council for Strategic research and was performed at the Competence Center for Catalysis, Chalmers University of Technology. The collaboration with Haldor Topsøe A/S, Amminex and DTU is gratefully acknowledged.

Notation

A = area for adsorption of one molecule
A_k = monolith wall area in tank k
$A(T)_j$ = temperature-dependent pre-exponential factor for reaction j
A_{ads} = pre-exponential factor for adsorption reactions
$c_{g,i,k}$ = concentration of species i in the gas phase of tank k
$c_{s,i,k}$ = concentration of species i on the surface of tank k
D = diffusivity
d_{channel} = channel diameter
E_a = activation energy
$E_a(0)$ = activation energy at zero surface coverage
$F_{i,k}$ = molar flow of species i in tank k
Gz = Graz number
H = Planck constant
k_B = Boltzmann constant
$k_{c,i,k}$ = mass-transfer coefficient of species i in tank k
k_j = rate constant for reaction j
L_{monolith} = length of monolith sample
M = molar mass
$m_{wc,k}$ = mass of washcoat in tank k
N_A = Avogadro's constant
N_{cat} = number of active sites per mass washcoat
$S(0)$ = Sticking coefficient
R = gas constant
$r_{j,k}$ = rate of reaction j in tank k
Sh = Sherwood number
T = temperature
v = linear gas velocity in the monolith channel

Greek letters

α_i = coverage dependence for species i
$\upsilon_{i,j}$ = Reaction coefficient of species i in reaction j
θ_{Sx} = Coverage of adsorption site Sx

Literature Cited

1. Sun Q, Gao ZX, Chen HY, Sachtler WMH. Reduction of NO_x with ammonia over Fe/MFI: Reaction mechanism based on isotopic labeling. *J Catal*. 2001;201(1):89–99.
2. Sjövall H, Olsson L, Fridell E, Blint RJ. Selective catalytic reduction of NO_x with NH_3 over Cu-ZSM-5 - The effect of changing the gas composition. *Appl Catal B Environ*. 2006;64(3-4):180–188.
3. Kwak JH, Tonkyn RG, Kim DH, Szanyi J, Peden CHF. Excellent activity and selectivity of Cu-SSZ-13 in the selective catalytic reduction of NO_x with NH_3. *J Catal*. 2010;275(2):187–190.
4. Uddin MA, Komatsu T, Yashima T. Catalytic properties of framework Fe_3^+ in MFI-type ferrisilicate - Reaction-mechanism studies of co oxidation using an isotopic tracer technique. *J Catal*. 1994; 146(2):468–475.
5. Richter M, Fricke R, Eckelt R. Unusual activity enhancement of NO conversion over Ag/Al_2O_3 by using a mixed NH_3/H_2 reductant under lean conditions. *Catal Lett*. 2004;94(1-2):115–118.
6. Doronkin DE, Fogel S, Tamm S, et al. Study of the "Fast SCR"-like mechanism of H_2-assisted SCR of NO_x with ammonia over Ag/Al_2O_3. *Appl Catal B Environ*. 2012;113-114:228–236.
7. Kondratenko EV, Kondratenko VA, Richter M, Fricke R. Influence of O_2 and H_2 on NO reduction by NH_3 over Ag/Al_2O_3: A transient isotopic approach. *J Catal*. 2006;239(1):23–33.
8. Breen JP, Burch R. A review of the effect of the addition of hydrogen in the selective catalytic reduction of NO_x with hydrocarbons on silver catalysts. *Top Catal*. 2006;39(1-2):53–58.
9. Brosius R, Arve K, Groothaert MH, Martens JA. Adsorption chemistry of NO_x on Ag/Al_2O_3 catalyst for selective catalytic reduction of NO_x using hydrocarbons. *J Catal*. 2005;231(2):344–353.
10. Chansai S, Burch R, Hardacre C, Breen J, Meunier F. Investigating the mechanism of the H_2-assisted selective catalytic reduction (SCR) of NO_x with octane using fast cycling transient in situ DRIFTS-MS analysis. *J Catal*. 2010;276(1):49–55.
11. Shibata J, Takada Y, Shichi A, Satokawa S, Satsuma A, Hattori T. Ag cluster as active species for SCR of NO by propane in the presence of hydrogen over Ag-MFI. *J Catal*. 2004;222(2):368–376.
12. Breen JP, Burch R, Hardacre C, Hill CJ. Structural investigation of the promotional effect of hydrogen during the selective catalytic reduction of NO_x with hydrocarbons over Ag/Al_2O_3 catalysts. *J Phys Chem B*. 2005;109(11):4805–4807.
13. Kannisto H, Ingelsten HH, Skoglundh M. Aspects of the role of hydrogen in H_2-assisted HC-SCR over Ag-Al_2O_3. *Top Catal*. 2009; 52(13-20):1817–1820.
14. Sazama P, Capek L, Drobna H, et al. Enhancement of decane-SCR-NO_x over Ag/alumina by hydrogen. Reaction kinetics and in situ FTIR and UV-vis study. *J Catal*. 2005;232(2):302–317.
15. Shibata J, Shimizu K, Satokawa S, Satsuma A, Hattori T. Promotion effect of hydrogen on surface steps in SCR of NO by propane over alumina-based silver catalyst as examined by transient FTIR. *Phys Chem Chem Phys*. 2003;5(10):2154–2160.
16. Zhang XL, Yu YB, He H. Effect of hydrogen on reaction intermediates in the selective catalytic reduction of NO_x by C_3H_6. *Appl Catal B Environ*. 2007;76(3-4):241–247.
17. Burch R, Breen JP, Hill CJ, et al. Exceptional activity for NO_x reduction at low temperatures using combinations of hydrogen and higher hydrocarbons on Ag/Al_2O_3 catalysts. *Top Catal*. 2004;30-31(1-4):19–25.
18. Meunier FC, Breen JP, Zuzaniuk V, Olsson M, Ross JRH. Mechanistic aspects of the selective reduction of NO by propene over alumina and silver-alumina catalysts. *J Catal*. 1999;187(2):493–505.
19. Creaser D, Kannisto H, Sjöblom J, Ingelsten HH. Kinetic modeling of selective catalytic reduction of NO_x with octane over Ag-Al_2O_3. *Appl Catal B Environ*. 2009;90(1-2):18–28.
20. Shimizu K, Shibata J, Satsuma A. Kinetic and in situ infrared studies on SCR of NO with propane by silver/alumina catalyst: Role of H_2 on O_2 activation and retardation of nitrate poisoning. *J Catal*. 2006; 239(2):402–409.
21. Guo Y, Chen J, Kameyama H. Promoted activity of the selective catalytic reduction of NO_x with propene by H_2 addition over a metal-monolithic anodic alumina-supported Ag catalyst. *Appl Catal A Gen*. 2011;397(1-2):163–170.
22. Tamm S, Valim N, Olsson L. The influence of hydrogen on nitrates during H_2-assisted SCR over Ag/Al_2O_3 catalysts - a DRIFT study. In press.
23. Tamm S, Fogel S, Gabrielsson P, Skoglundh M, Olsson L. The effect of the gas composition on hydrogen assisted NH_3-SCR over Ag/Al_2O_3. *Appl Catal B Environ*. 2013;136-137:168–176.
24. Sjövall H, Blint RJ, Gopinath A, Olsson L. A Kinetic model for the selective catalytic reduction of NO_x with NH_3 over an Fe-zeolitecatalyst. *Ind Eng Chem*. 2010;49(1):39–52.
25. Lindholm A, Currier NW, Li JH, Yezerets A, Olsson L. Detailed kinetic modeling of NO_x storage and reduction with hydrogen as the reducing agent and in the presence of CO_2 and H_2O over a Pt/Ba/Al catalyst. *J Catal*. 2008;258(1):273–288.
26. Colombo M, Nova I, Tronconi E, Schmeisser V, Bandl-Konrad B, Zimmermann L. $NO/NO_2/N_2O$-NH_3 SCR reactions over a commercial Fe-zeolite catalyst for diesel exhaust aftertreatment: Intrinsic kinetics and monolith converter modelling. *Appl Catal B Environ*. 2012;111:106–118.
27. Nova I, Colombo M, Tronconi E, Schmeisser V, Weibel M. The NH_3 Inhibition effect in the standard scr reaction over a commercial Fe-zeolite catalyst for diesel exhaust aftertreatment: an experimental and modeling study. *SAE Int J Engines*. 2011;4(1):1822–1838.
28. Backman H, Arve K, Klingstedt F, Murzin DY. Kinetic considerations of H_2 assisted hydrocarbon selective catalytic reduction of NO over Ag/Al_2O_3 - II. *Kinetic modelling*. *Appl Catal A Gen*. 2006; 304(1):86–92.
29. Mhadeshwar AB, Winkler BH, Eiteneer B, Hancu D. Microkinetic modeling for hydrocarbon (HC)-based selective catalytic reduction (SCR) of NO_x on a silver-based catalyst. *Appl Catal B Environ*. 2009;89(1-2):229–238.
30. Sawatmongkhon B, Tsolakis A, Theinnoi K, York APE, Millington PJ, Rajaram RR. Microkinetic modelling for selective catalytic reduction (SCR) of NO_x by propane in a silver-based automotive catalytic converter. *Appl Catal B Environ*. 2012;111-112:165–177.
31. Boudart M, Djega-Mariadassou G. Kinetics of Heterogeneous Catalytic Reactions. Princeton, NJ: Princeton University Press; 1984.
32. Olsson L, Sjövall H, Blint RJ. Detailed kinetic modeling of NO_x adsorption and NO oxidation over Cu-ZSM-5. *Appl Catal B Environ*. 2009;87(3-4):200–210.
33. Dumesic JA, Rudd DF, Aparicio LM, Rekoske JE, Treviño AA, eds. The Microkinetics of Heterogeneous Catalysis. Washington, DC: American Chemical Society; 1993. ACS Professional Reference Book.
34. Fuller EN, Schettle PD, Giddings JC. A new method for prediction of binary gas-phase diffusion coeffecients. *Ind Eng Chem*. 1966; 58(5):19–27.
35. Knözinger H, Ratnasamy P. Catalytic aluminas - surface models and characterization of surface sites. *Catal Rev Sci Eng*. 1978;17(1):31–70.
36. Digne M, Sautet P, Raybaud P, Euzen P, Toulhoat H. Use of DFT to achieve a rational understanding of acid-basic properties of gamma-alumina surfaces. *J Catal*. 2004;226(1):54–68.
37. Hellman A, Groünbeck H. First-Principles Studies of NO_x Chemistry on Ag_n/α-Al_2O_3. *J Phys Chem. C*. 2009;113(9):3674–3682.
38. Wilken N, Kamasamudram K, Currier NW, Li J, Yezerets A, Olsson L. Heat of adsorption for NH_3, NO_2 and NO on Cu-Beta zeolite using microcalorimeter for NH_3-SCR applications. *Catal Today*. 2010;151(3-4):237–243.
39. Saha D, Deng SG. Characteristics of ammonia adsorption on activated alumina. *J Chem Eng Data*. 2010;55(12):5587–5593.
40. Sjövall H, Blint RJ, Olsson L. Detailed kinetic modeling of NH_3 SCR over Cu-ZSM-5. *Appl Catal B Environ*. 2009;92(1-2):138–153.
41. Li WX, Stampfl C, Scheffler M. Insights into the function of silver as an oxidation catalyst by ab initio atomistic thermodynamics. *Phys Rev B*. 2003;68(16).

Manuscript received Feb. 18, 2013, and revision received May. 6, 2013.